Pergamon

Int. J. Solids Structures Vol. 34, No. 1, pp. 19–30, 1997

0020 7683/97 $15.00 + .00

0020–7683(95)00288–X

APPLICATIONS OF THE GREEN FUNCTION FOR A HALF CIRCULAR CRACK

GUIDO DHONDT
MTU Motoren- und Turbinen-Union München GmbH, Postfach 50 06 40, 80976 München, Germany

(*Received* 28 *July* 1995; *in revised form* 29 *November* 1995)

Abstract—The stress intension factor (K) distribution along a half circular crack in half infinite space due to arbitrary mode I loading is derived based on the Green function solution developed in a previous article. Using a perturbation theory first introduced by Rice, the theory is extended to somewhat half circular cracks. This technique allows for the cycle by cycle calculation of arbitrarily shaped surface cracks subject to an arbitrary mode I stress distribution. Several examples show the field and limits of application. Copyright © 1996 Elsevier Science Ltd

1. INTRODUCTION

In a previous article (Dhondt, 1995) the Green functions were derived for a half circular crack in a half space under normal loading for about sixty representative point load positions. They represent fundamental solutions, which can be used in a wide variety of applications.

The most evident application is the calculation of the stress intensity factor (K) distribution along a half circular crack in a half space subject to arbitrary mode I loading. To this end the Green functions, weighted by the actual load, are integrated over the crack area. This requires the knowledge of the Green function at every point, which was achieved by linear interpolation within a Delaunay triangulation of the available point load set. The results are compared with the literature (Pickard, 1986).

An extension to K-calculations along not quite half circular surface cracks can be obtained by using a perturbation theory developed by Rice (1989). This technique establishes a link between a perturbation of a crack front for which the K-values are known and the change in K due to this perturbation and is intimately connected with the knowledge of the Green functions for the unperturbed crack. Application of the theory to half elliptical cracks illustrates its use and limitations.

A further step along the same line naturally leads to the cycle by cycle calculation of the crack propagation of a surface crack subject to arbitrary loading. This is especially interesting for initial cracks which are not half circular, e.g., due to an inclusion, or non constant stress fields, e.g., obtained by surface treatment such as shot peening.

2. K-DISTRIBUTION FOR ARBITRARY LOADING

In a previous publication (Dhondt, 1995) the Green functions were obtained for a half circular crack in half infinite space for a set of representative point load positions. This information can be used to find the K-distribution due to an arbitrary loading. To this end it is necessary to know the K-distribution due to a point load at an arbitrary position. This can be achieved by performing a Delaunay triangulation (Sloan and Houlsby, 1983) on the discrete set of available point load positions followed by linear interpolation.

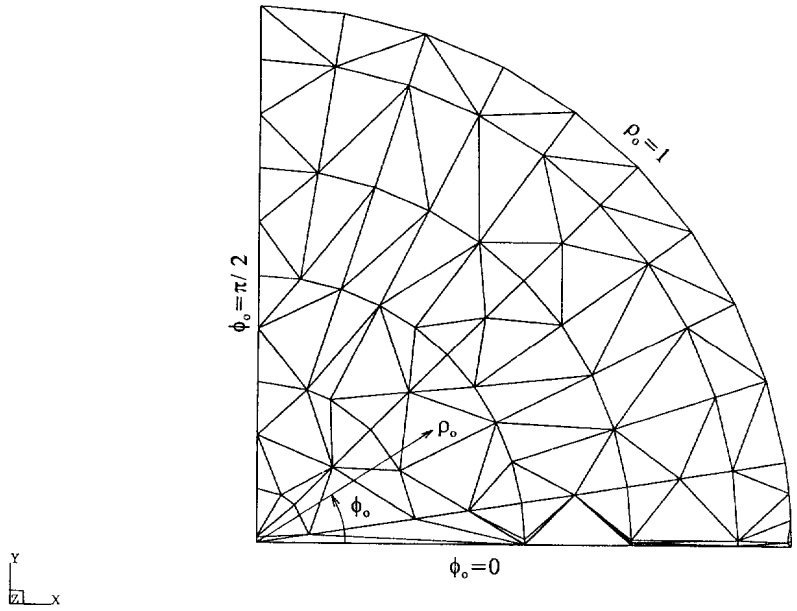

Fig. 1. Triangulation of the point load positions.

In Dhondt (1995) it is shown that the K-value $K(\phi)$ at position ϕ along the crack front ($0 \leqslant \phi \leqslant \pi$) due to a unit compressive point load at (ρ_o, ϕ_o) (Fig. 1) takes the form

$$K(\phi) = K(\phi)_0 + K(\phi)_1 \tag{1}$$

where

$$K(\phi)_0 = \frac{1}{\pi\sqrt{\pi a}}\sqrt{a^2-\rho_0^2}\left(\frac{1}{r_1^2}+\frac{1}{r_2^2}\right) \tag{2}$$

$$K(\phi)_1 = \alpha(\phi) + \left(\frac{2}{\pi}\right)^{7/2} \frac{vF(v)\sqrt{a^2-\rho_0^2}\ln(\sin(\phi))}{(a^2+\rho_0^2-2a\rho_0\cos\phi_0\cos\phi)\sqrt{2a}} + \left[C_0 + \frac{C_\pi - C_0}{\pi}\phi\right] \tag{3}$$

and

$$r_{1,2}^2 = a^2+\rho_0^2-2a\rho_0\cos(\phi\pm\phi_0) \tag{4}$$

$$F(v) = 0.1788+0.3856v \tag{5}$$

where a is the radius of the crack, v is Poisson's coefficient, $\alpha(\phi)$, C_0 and C_π are functions of the point load position and are given in Dhondt (1995) for a representative set of positions. The above formulas were obtained as the result of an iteration process in which $K(\phi)_0$ represents the zero order solution (full circular crack loaded by two symmetrical forces) and $K(\phi)_1$ represents the first correction. Position '$K5$' was dropped since it yields incorrect results. To be able to cover every position within the half circular crack the set of point load positions was complemented by selected positions along the boundary $\rho_0 = 1$ and the boundary $\phi_0 = 0$. $K(\phi)_1 = 0$ for $\rho_0 = 1$. At the free boundary $\phi_0 = 0$ the $K(\phi)_1$ values in the few available point load positions a distance $10^{-3}\cdot a$ away from the free boundary were projected onto the boundary. The resulting Delaunay triangulation is shown in Fig. 1.

Switching to carthesian coordinates x, y and focusing on one Delaunay triangle i, let the vertices be denoted by (x_{1i}, y_{1i}), (x_{2i}, y_{2i}), (x_{3i}, y_{3i}) and the Green functions for each of the vertices by $K_{1i}(\phi)$, $K_{2i}(\phi)$ and $K_{3i}(\phi)$. Then the K-distribution for a point force within the triangle can be expressed by a linear interpolation:

$$K_i(\phi; x, y) = a_i(\phi)x + b_i(\phi)y + c_i(\phi) \tag{6}$$

where a_i, b_i and c_i satisfy

$$\begin{cases} a_i(\phi)x_{1i} + b_i(\phi)y_{1i} + c_i(\phi) = K_{1i}(\phi) \\ a_i(\phi)x_{2i} + b_i(\phi)y_{2i} + c_i(\phi) = K_{2i}(\phi) \\ a_i(\phi)x_{3i} + b_i(\phi)y_{3i} + c_i(\phi) = K_{3i}(\phi) \end{cases} \tag{7}$$

The solution of this set of equations yields:

$$\begin{cases} a_i(\phi) = \dfrac{1}{D_i}[a_{1i}K_{1i}(\phi) + a_{2i}K_{2i}(\phi) + a_{3i}K_{3i}(\phi)] \\ b_i(\phi) = \dfrac{1}{D_i}[b_{1i}K_{1i}(\phi) + b_{2i}K_{2i}(\phi) + b_{3i}K_{3i}(\phi)] \\ c_i(\phi) = \dfrac{1}{D_i}[c_{1i}K_{1i}(\phi) + c_{2i}K_{2i}(\phi) + c_{3i}K_{3i}(\phi)] \end{cases} \tag{8}$$

where

$$\begin{aligned} a_{1i} &= y_{2i} - y_{3i} \\ b_{1i} &= x_{3i} - x_{2i} \\ c_{1i} &= x_{2i}y_{3i} - y_{2i}x_{3i} \\ D_i &= c_{1i} + c_{2i} + c_{3i} \end{aligned} \tag{9}$$

complemented by appropriate cyclic permutations of the indices. The K-distribution due to an arbitrary loading $p(x, y)$ can now be expressed by

$$K(\phi) = \sum_i \int_{\Delta_i} p(x, y)K_i(\phi; x, y)\,\mathrm{d}x\,\mathrm{d}y \tag{10}$$

where Δ_i denotes triangle i. Substitution of eqn (6) into eqn (10) finally yields:

$$K(\phi) = \sum_i [a_i(\phi)I_{ix} + b_i(\phi)I_{iy} + c_i(\phi)I_i] \tag{11}$$

where

$$I_{ix} = \int_{\Delta_i} xp(x, y)\,\mathrm{d}x\,\mathrm{d}y \tag{12}$$

$$I_{iy} = \int_{\Delta_i} yp(x, y)\,\mathrm{d}x\,\mathrm{d}y \tag{13}$$

$$I_i = \int_{\Delta_i} p(x, y)\,\mathrm{d}x\,\mathrm{d}y \tag{14}$$

are the only load dependent quantities.

3. A HALF CIRCULAR CRACK SUBJECT TO A LINEAR STRESS GRADIENT

The theory of the previous section was applied to the problem of a half circular crack subject to a stress distribution σ_{zz} of the form

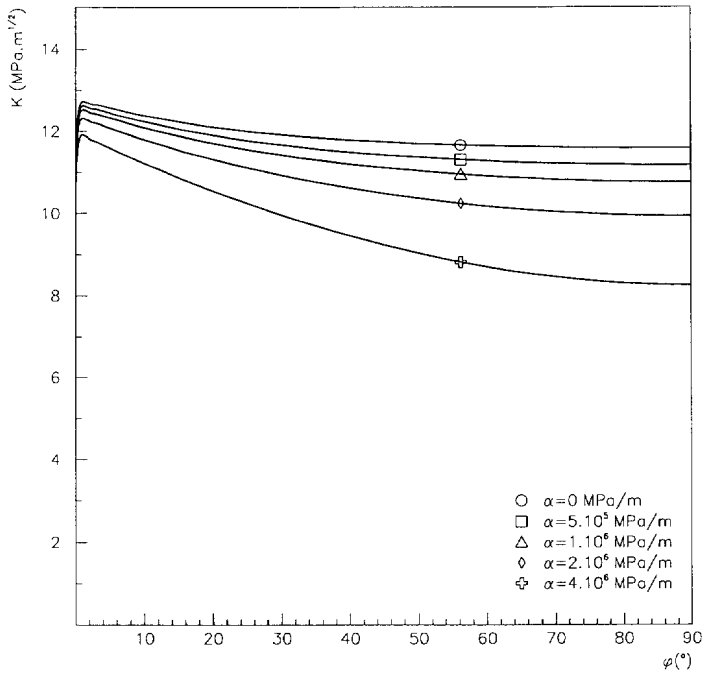

Fig. 2. K-distribution along a half circular crack subject to a linear stress gradient.

$$\sigma_{zz}(\text{MPa}) = 1000 \cdot -\alpha y(m) \tag{15}$$

where y is the carthesian coordinate perpendicular to the free surface, z is perpendicular to the crack faces and m stands for metre. The radius of the crack was 10^{-4} m and the stress at the free surface was 1000 MPa. Figure 2 shows the K-distribution along half the crack (0° (free surface) $\leqslant \phi \leqslant 90^\circ$ (deepest point)) for different values of α.

It is noticed that K generally increases towards the free surface. However, at the free surface there is a sharp drop leading to an extremely small boundary layer. This behaviour is the natural extension of the same phenomenon already noticed for the Green functions. It leads to a zero K-value very close to the free surface (10^{-13} times the crack length). For increasing values of α the K-values at $\phi = 90^\circ$ linearly decrease whereas the maximum K-value along the crack front doesn't change much.

The K-values at $\phi = 0^\circ$ and $\phi = 90^\circ$ for different values of α are collected in Table 1 and compared with values obtained by the Finite Element Method (Pickard, 1986). Whereas the values at $\phi = 90^\circ$ match perfectly, the Green function values at the local maximum near $\phi = 0^\circ$ are slightly smaller than the Pickard results. Evidently, the Finite Element Method cannot cope with the extremely small boundary layer and thus the distribution, instead of dropping at the free surface, continues to increase. Indeed, if the local maximum values are extrapolated towards the free surface they come very close to the Pickard results, especially for higher values of α.

Table 1. K-values (MPa · m$^{1/2}$) along a half circular crack subject to a linear stress gradient

	$\phi = 0^\circ$		$\phi = 90^\circ$	
α (MPa/m)	Green function	Pickard	Green function	Pickard
0	12.72	12.91	11.60	11.61
$5 \cdot 10^5$	12.62	12.80	11.18	11.19
$1 \cdot 10^6$	12.52	12.68	10.76	10.78
$2 \cdot 10^6$	12.32	12.45	9.93	9.94
$4 \cdot 10^6$	11.92	11.99	8.27	8.28
$5 \cdot 10^6$	11.72	11.76	7.44	7.44

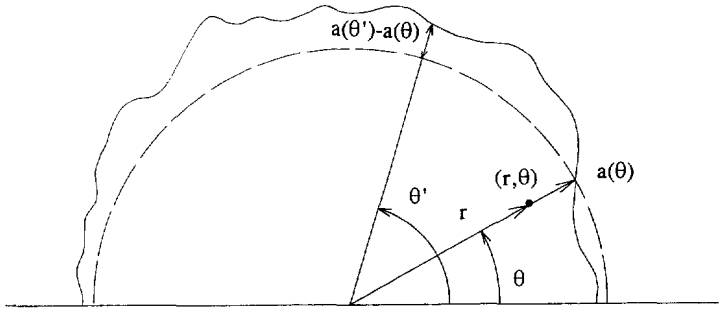

Fig. 3. Geometric configuration for a somewhat half circular crack.

4. K-DISTRIBUTION FOR SOMEWHAT HALF-CIRCULAR CRACKS

In Gao and Rice (1987) a formula is derived which expresses the change in crack opening displacement for a somewhat circular crack due to a deviation from the perfect circular form. Apart from the integration range this formula also holds for a somewhat half circular crack and reads

$$\delta[\Delta u(r,\theta)] = \frac{2(1-\nu^2)}{E}\int_0^{\pi} K^0[\theta';a(\theta)]\cdot a(\theta)\cdot k[\theta';r,\theta;a(\theta)]\cdot[a(\theta')-a(\theta)]\,\mathrm{d}\theta' \qquad (16)$$

where (Fig. 3) $\Delta u(r,\theta)$ is the crack opening displacement at position (r,θ) and $\delta[\Delta u(r,\theta)]$ expresses the change in $\Delta u(r,\theta)$ due to the perturbation of the original half circular crack shape with radius $a(\theta)$. $K^0[\theta';a(\theta)]$ and $k[\theta';r,\theta;a(\theta)]$ are the stress intensity factors at θ' along a perfectly half circular crack with radius $a(\theta)$ subject to the actual load and a unit force at (r,θ), respectively, and E is Young's modulus. $K^0[\theta';a(\theta)]$ has been derived in Section two of the present article. Equation (16) is exact to first order in $a(\theta')-a(\theta)$.

The derivation of the Green functions in Dhondt (1995) has shown that the relationship between the stress intensity factor and the crack opening displacement at any point along the crack front is, apart from locations extremely close to the free surface, essentially a plane strain configuration satisfying:

$$\Delta u(r,\theta) \sim \frac{8(1-\nu^2)}{E}K\sqrt{\frac{a-r}{2\pi}}, \quad r\to a \qquad (17)$$

Furthermore, the Green function along a half circular crack coincides with the Green function for a full circular crack for $r\to a$, except exactly at the free boundary. After substitution of eqn (17) into eqn (16) this leads to (Gao and Rice, 1987):

$$\delta K(\theta) = \frac{1}{8\pi}PV\int_0^{\pi}\frac{K^0[\theta';a(\theta)]\cdot[a(\theta')/a(\theta)-1]}{\sin^2[(\theta'-\theta)/2]}\mathrm{d}\theta' \quad \theta\neq 0,\pi \qquad (18)$$

where PV denotes the Principal Value. The total stress intensity value $K(\theta)$ is expressed by $K(\theta) = K^0[\theta,a(\theta)]+\delta K(\theta)$. Thus, to calculate the K-factor at position θ a half circular crack with radius $a(\theta)$ is considered (Fig. 3). Then the K-value at θ along this half circular crack shape due to the actual loading, i.e., $K^0[\theta,a(\theta)]$ is calculated. Finally $\delta K(\theta)$ is obtained by integration along the half circular crack using eqn (18) and added to $K^0[\theta,a(\theta)]$.

5. HALF ELLIPTICAL CRACKS SUBJECT TO CONSTANT STRESS

The theory of the previous section was applied to a variety of half elliptical cracks. About 20 equidistant points were chosen along the crack front at which K was calculated. To avoid problems at $\phi = 0, \pi$ (cf. eqn (18)), the first and last sampling point were set at

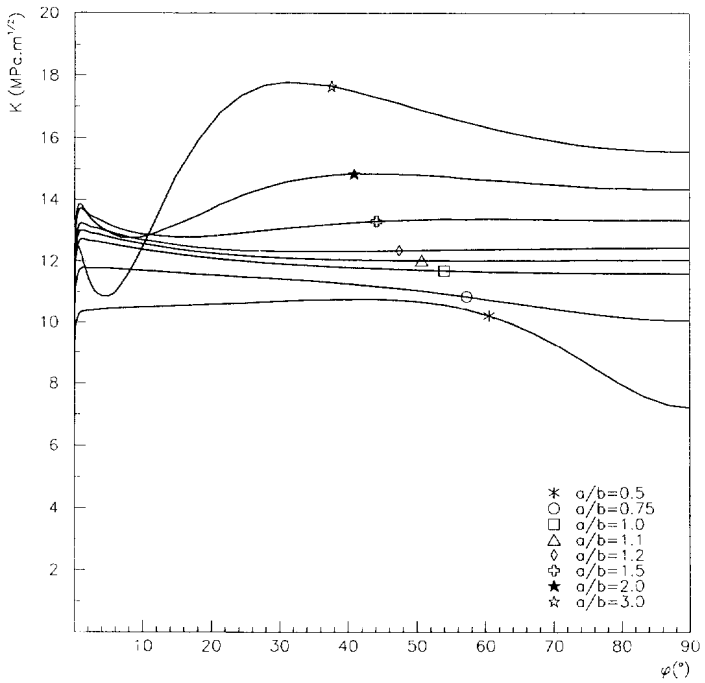

Fig. 4. K-distribution along half elliptical cracks subejct to constant stress.

$\phi = 10^{-6}$ and $\phi = \pi - 10^{-6}$ respectively. The depth b of the crack was fixed at 0.1 mm. The ratio of the axis a along the free boundary to b ranged from 0.33 to 3.

The K-distribution for ratios between 0.5 and 3 and a constant stress of 1000 MPa is shown in Fig. 4 All curves exhibit a boundary layer at $\phi = 0°$. For increasingly shallow cracks the K-distribution generally increases and two maxima are created at about $\phi = 35°$ and $\phi = 145°$ with a local minimum in between at $\phi = 90°$. In Fig. 5 the result for $a/b = 2$ is compared with the K-distribution obtained by using the Pickard formulas (Pickard, 1986). The Pickard distribution was obtained by multiplying the K values for $a/b = 1$ by (see also Gao and Rice, 1987):

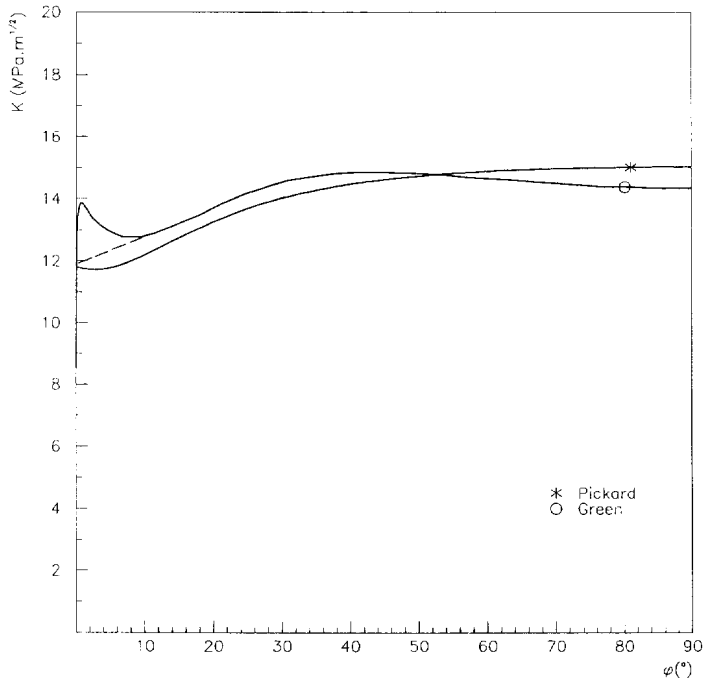

Fig. 5. Comparison between the present results and the K-distribution obtained by Pickard.

Table 2. K-values at $\phi = 90^\circ$

a/b (−)	K(Pickard) (MPa·m$^{1/2}$)	K(Green) (MPa·m$^{1/2}$)	Deviation (%)
0.20	3.47	−1.29	−368.6
0.33	5.41	4.02	34.7
0.50	7.52	7.22	4.2
0.75	9.89	10.05	1.6
1.00	11.61	11.61	0.0
1.10	12.15	12.04	0.9
1.20	12.63	12.43	1.6
1.50	13.78	13.32	3.5
2.00	15.05	14.34	4.9
3.00	16.37	15.56	5.2
5.00	17.36	16.93	2.5

$$f(\phi) = \frac{\sqrt{2.464}}{E(k)} \left[\frac{\cos^2 \phi + k^4 \sin^2 \phi}{\cos^2 \phi + k^2 \sin^2 \phi} \right]^{1/4} \tag{19}$$

where $k = a/b = 2$, $E(k)$ is the complete elliptic integral of the second kind as defined by Pickard (1986) and ϕ starts at the free boundary. The function $f(\phi)$ is a correction factor which accounts for the ellipticity of the crack. It is exact for elliptical subsurface cracks and Pickard showed that, when applied to elliptical surface cracks, the deviation from Finite Element results stays within 3% for $0.5 \leqslant k \leqslant 2$.

Both curves are qualitatively similar. The two main differences are the absence of the local minimum at $\phi = 90^\circ$ and the absence of the boundary layer at $\phi = 0^\circ$ in the Pickard solution. Since the basic Pickard solution was obtained by means of Finite Element calculations it is quite clear that the extremely thin boundary layer is missed. However, continuing the present solution from about $\phi = 10^\circ$ to the free boundary yields values very close to the Pickard ones (broken line), i.e., it looks as if the boundary layer solution is superimposed on the Finite Element results within a small layer at the free surface. The presence at $\phi = 90^\circ$ of a local minimum in the Green function solution can be considered as a remnant of the basic $a/b = 1$ solution. There is no compelling reason why this minimum should remain in place for $a/b \gg 1$ and in this region the Pickard solution is probably the more accurate one. In Table 2 the K-values at the deepest point ($\phi = 90^\circ$) are compared

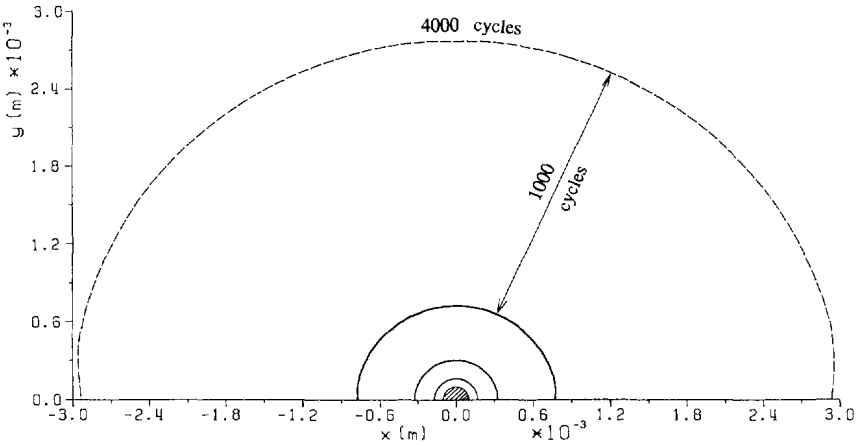

Fig. 6. Crack propagation of a half circular crack subject to constant stress.

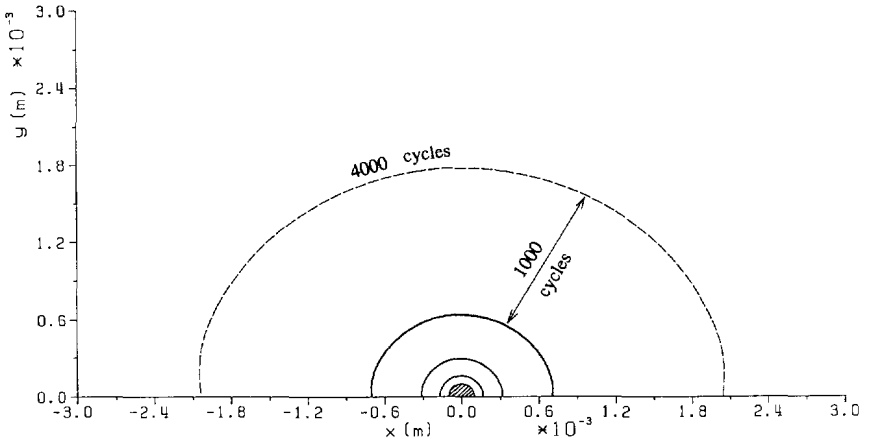

Fig. 7. Crack propagation of a half circular crack subject to a linearly decreasing stress field $\sigma_{zz} = 1000\text{-}10^5\ y$ (MPa).

for several a/b ratios. Within the validated Pickard range ($0.5 \leqslant a/b \leqslant 2$) the deviation defined as

$$\text{Dev} = \frac{K(\text{Pickard}) - K(\text{Green})}{K(\text{Green})} \tag{20}$$

grows monotonically for increasing $|a/b - 1|$ values, but stays within 5%. The values for the other ratios show the Green function solution might not be applicable for $a/b \leqslant 0.5$.

6. CYCLIC CRACK PROPAGATION CALCULATIONS FOR SURFACE CRACKS

One of the major challenges in fracture mechanics is the reliable prediction of the propagation of initial cracks subject to complex stress fields. This includes the ability to predict the actual position and shape of the crack at any stage of the propagation process. Focusing on surface cracks subject to mode I loading this requires the determination of the

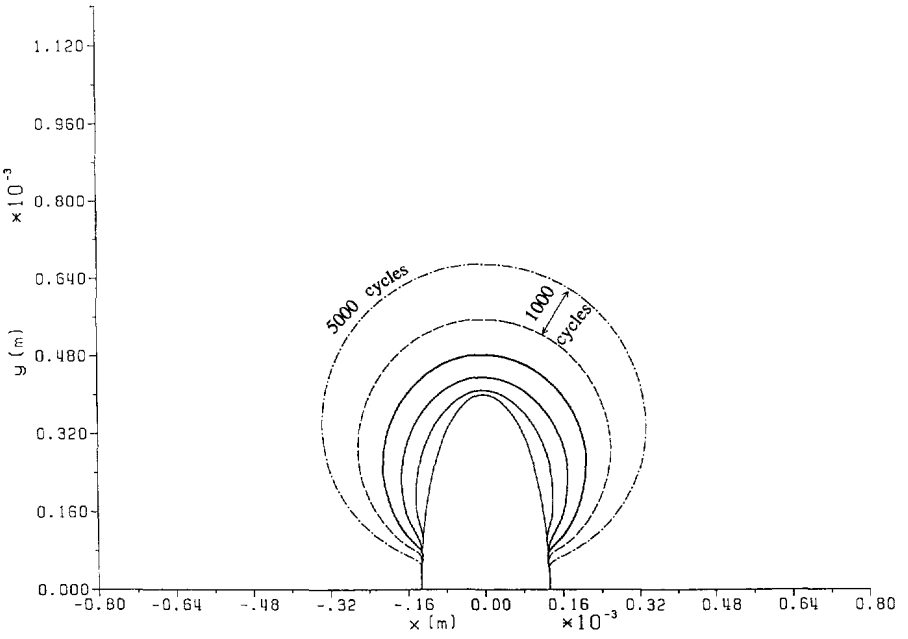

Fig. 8. Simulation of the crack propagation at a nonmetallic inclusion.

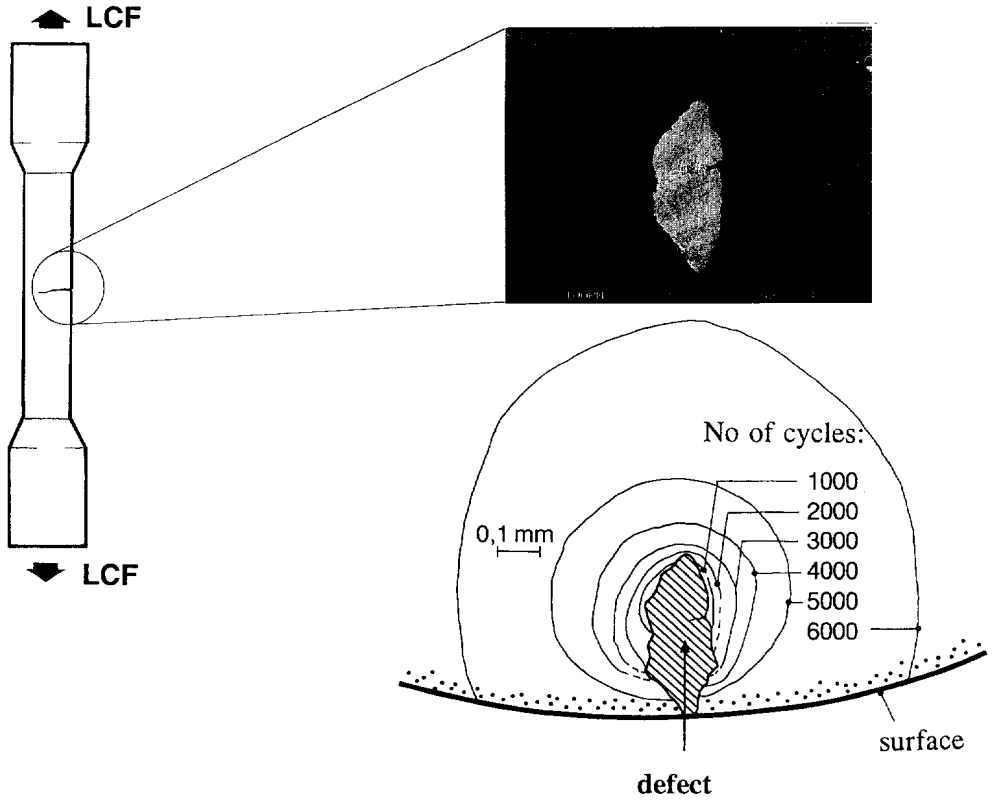

Fig. 9. Experimentally determined crack propagation at a nonmetallic inclusion.

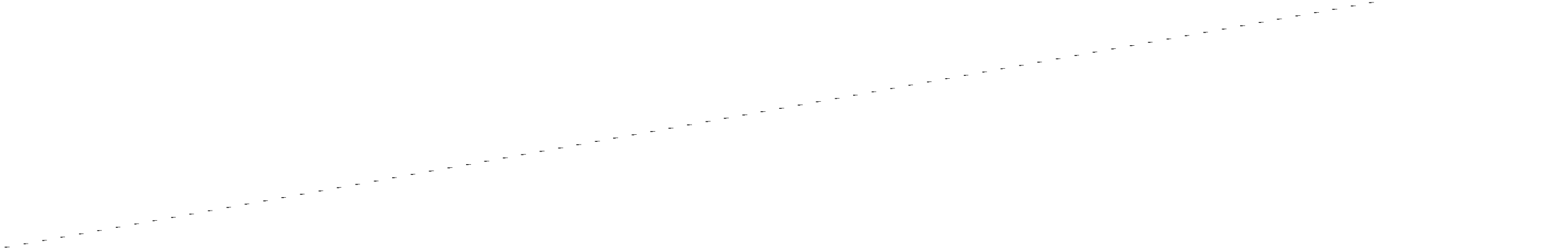

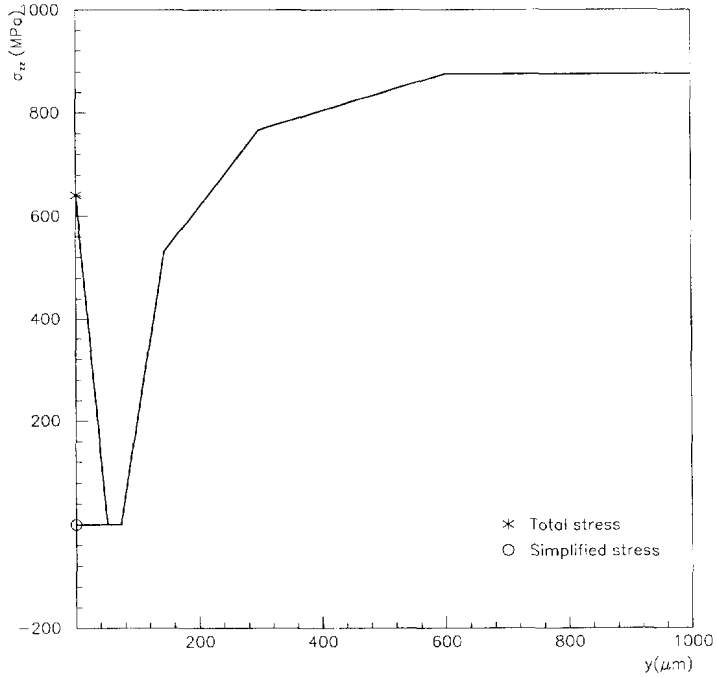

Fig. 10. Stress profile at the free boundary as a function of depth.

K-distribution along a somewhat half circular crack subject to an arbitrary stress field. This is exactly the problem solved in Section 4. Repeated calculation of the K-distribution allows for a cycle by cycle crack propagation calculation. This procedure was successfully applied to subsurface cracks in a previous publication (Dhondt, 1994).

In the applications in this section a new K-calculation was performed every 20 cycles. The crack propagation was calculated by means of a Paris type law and was assumed to be orthogonal towards the local crack front except at the free surface where the propagation was taken parallel to the surface.

Figure 6 shows the crack propagation of an initially half circular crack with radius 0.1 mm (hatched area) subject to a constant load $\sigma_{zz} = 1000$ MPa. The new crack front was plotted every 1000 cycles. At the free boundary it is observed that the crack lags behind, a phenomenon which is well known from experiments. Although this behaviour is frequently attributed to plasticity effects at the free boundary, in the present linear elastic calculations it is naturally due to the boundary layer in the K-distribution. Since the K-values have a local minimum at $\phi = 90°$, the crack has the tendency to propagate slightly faster along the free boundary. After 4000 cycles a/b (a is measured along the free surface, b is the maximum crack depth) is about 1.05. This effect is naturally stronger for a stress distribution which decreases linearly with depth (Fig. 7). Here σ_{zz} drops from 1000 MPa at the free surface to 900 MPa at a depth of 1 mm. After 4000 cycles a/b attains a value of 1.15.

Figure 8 shows the simulation of crack propagation starting from an artificially introduced defect in a Low Cycle Fatigue specimen. The experimental results of this test (Nowak and König, 1988; König and Bergmann, 1992) are depicted in Fig. 9. In this test the position of the crack front at increments of 1000 cycles was monitored by a marker load technique (König and Affeldt, 1987). The surface of the specimen was shot peened leading to a significant residual stress field. The superposition of the residual stresses and the stress field due to the test load is represented by the solid line in Fig. 10. For the calculations this stress profile was simplified by removing the local maximum at the free surface. Since the starting crack, which coincides with the initial defect, is rather deep, this surface layer does not have much influence and the removal leads to a much faster convergence of the integration routines. The true geometry of the initial defect is extremely complicated and has been modelled by a semi-elliptical crack with ratio of the axes 1 : 3. Table 2 indicates that this is very near to the limits of the envelope of applicability of the present method.

Nevertheless, a comparison of Figs 8 and 9 shows that the numerical results are qualitatively very similar to the experimental evidence. The crack starts to propagate at the interior of the specimen and attains a nearly circular shape before propagating towards the free surface. Because of the complicated intermediate geometries and stress field a new K-calculation was performed only every 100 cycles and the calculation was stopped after 5000 cycles. Yet it qualitatively illustrates that the Green function method is a potentially powerful method for complex geometries and loadings.

7. CONCLUSIONS

The K-distribution along a half circular crack in half infinite space subject to arbitrary loading was derived based on the Green function solution. The field of application was further extended to somewhat half circular cracks by applying a perturbation theory developed by Rice (1989). This allowed for the cycle by cycle calculation of surface cracks predicting the crack front shape and the corresponding number of load cycles. Numerous examples showed the strength and limits of this newly developed technique.

Acknowledgements—The author wishes to thank G. König for providing him with the Low Cycle Fatigue Specimen test data.

REFERENCES

Dhondt, G. (1994). Cyclic propagation of subsurface cracks. In *Proc. 10th Eur. Conf. on Fracture*, Berlin, September 20–23 1994, (eds K.H. Schwalbe and C. Berger) pp. 1239–1244.

Dhondt, G. (1995). Green functions for a half circular crack in half infinite space under normal loading. *Int. J. Solids Structures* **32,** 1807–1857.

Gao, H. and Rice, J. R. (1987). Somewhat circular tensile cracks. *Int. J. Fracture* **33,** 155–174.

König, G. W. and Affeldt, E. E. (1987). Experience with a load change technique for crack growth rate measurements. In *Proc. Conf. Low Cycle Fatigue and Elasto-Plastic Behaviour of Materials*, Munich, 7–11 September 1987, pp. 673–679.

König, G. W. and Bergmann, J. W. (1992) Predicting defect behaviour. *AGARD Report* 790: *Impact of Material Defects on the Engine Structural Integrity*.

Nowak, B. and König, G. W. (1988). Defect investigation in powder metallurgical nickel base alloys, MTU internal report.

Pickard, A. C. (1986). *The Application of 3-Dimensional Finite Element Methods to Fracture Mechanics and Fatigue Prediction*, Chameleon Press, London.

Rice, J. R. (1989). Weight function theory for three-dimensional elastic crack analysis. In *Fracture Mechanics: Perspectives and Directions* (Twentieth Symposium), ASTM STP 1020 (eds R.P. Wei and R.P. Gangloff), American Society for Testing and Materials, Philadelphia, pp. 29–57.

Sloan, S. W. and Houlsby, G. T. (1983). An implementation of Watson's algorithm for computing 2-dimensional Delaunay triangulations. *Solid Mechanics Report No. SM*045/83, University of Oxford, UK.